Automatic geometric digital twin of box girder bridge using a laser-scanned point cloud

Jiangpeng Shu [a,b,c], Ziyue Zeng [a,*], Wenhao Li [a], Shukang Zhou [a], Congguang Zhang [a], Caie Xu [d], He Zhang [a]

[a] College of Civil Engineering and Architecture, Zhejiang University, Hangzhou, 310058, China
[b] Innovation Center of Yangtze River Delta, Zhejiang University, Jiaxing, 314100, China
[c] Architectural Engineering Institute, Sanming University, Sanming, 365004, China
[d] School of Information and Electronic Engineering, Zhejiang University of Science and Technology, Hangzhou, 310023, China

ARTICLE INFO

ABSTRACT

Geometric modeling is a pivotal step in creating a digital twin for existing bridge structures. Its deficiency of automation makes geometric modeling step time-consuming and laborious. This paper presents a solution for automatically modeling box girder bridges, including external and internal structures, based on laser-scanned point cloud. The solution includes three vital methods: component segmentation, key points extraction of cross-section, and internal structure reconstruction. The results indicate that the established segmentation model, BCR-Net, exhibited better performance than PointNet++ in component segmentation, as demonstrated by mIoU of 0.9751 on the test set. The mean absolute error on the dimension of the pier, bent cap and external and internal structure of the box girder is 0.27 %, 0.38 %, 0.47 %, and 0.48 %, respectively. It means the proposed methods possessed excellent modeling accuracy while ensuring high efficiency than manual modeling, providing a promising solution for digital twin modeling of bridge structures.

1. Introduction

The box girder bridge, characterized by main beams comprising girders shaped like hollow boxes, which were popular from 1960s attributing to its notable advantages, such as lightweight, fast fabrication speed, low costs, excellent resistance to wind and torsion, and an aesthetically pleasing aspect essential for urban environments [1]. With the increase of service time, built box girder bridges may face potential structural risks. To keep the security of civil lives and property, its structure health evaluation is receiving increasing attention [2–6]. Constructing a digital twin (DT) is one of cutting-edge technology to structure health evaluation [7]. A DT is a virtual representation encompassing geometry, material characteristics, and defects, facilitating real-time data exchange between the physical structure and its virtual counterpart [8]. This technological innovation allows for predictive analysis of future conditions, thereby avoiding potential asset losses.

Geometric modeling generally is a first and most important step to construct a digital twin. The precision and efficiency of geometric modeling directly decides reliability and validity of predictive results from digital twin. Moreover, geometric modeling also is basic technology for Building Information Modeling (BIM) and Finite Element Analysis (FEA). These technologies are widely used in the construction industry to enhance project performance from design to construction and facilities management [9]. However, accurately and fastly acquiring modeling geometric parameter has been a significant challenge in geometric modeling for bridges.

The traditional method involves manually constructing a three-dimensional (3D) model based on design drawings, a process notorious for its time and labor intensity. One of the most noteworthy issues is that the traditional method disregards the deformation of the bridge during both construction and service. Namely, the model built by the traditional method is an as-design model rather than an as-built or as-is model [10]. In 2005, Kim et al. [11] explored a rapid modeling method to transform data collected by a laser range finder into decision-supporting information within a virtual model, which proved point cloud can provide accurate and fast records of 3D geometric information related to construction-related objects. Subsequently, with

* Corresponding author.
  E-mail addresses: Jpeshu@zju.edu.cn (J. Shu), Zengzy96@zju.edu.cn (Z. Zeng).

technological advancements, point clouds could be acquired from numerous sources, such as laser scans, images, and videos. Hence, it has become one of the primary data sources for 3D model reconstruction based on its advantages, including ease of acquisition and the ability to describe object geometrics effectively [12]. Point cloud research extends to different construction-related objects, including buildings [13–17], bridges and tunnels, and other civil infrastructures. Specifically, these are construction equipment and vehicles [18,19] in construction sites, furniture [20], and pipelines [21] in buildings and bridges [22–24]. Therefore, 3D reconstruction from point cloud data could effectively address the bridge's disregarded deformation in construction and service.

Geometric modeling based on point clouds encompasses several vital steps, including pre-processing, segmentation, geometric feature extraction, and model creation [25]. Pre-processing refers to the cleanup and registration of raw data points, and this stage is relatively well-established. The segmentation step focuses on labeling point clouds into object categories, such as bridge slab, pier, and box girder. In recent years, attention has been dedicated to addressing this challenge by presenting accurate automatic segmentation methods.

The region-growing method was proposed for automatically segmenting components and classifying point cloud data from bridges [26–28]. This method involves classifying point clouds into different categories by controlling a threshold for the change in normal vectors when seed points extend to the edge of a region. However, a limitation of this method is that the seed point and threshold are either manually specified or determined automatically under specific conditions. Besides, another technique involving geometric shape descriptors [29] also relies heavily on manually designing descriptors and adjusting their parameters for segmentation. Schnabel et al. [30] introduced an automatic method based on random sample consensus (RANSAC), where randomly extracted samples from the point cloud data are compared with a 3D geometry model (such as a sphere or cylinder). The model was built where the sum of distances is minimized. Nevertheless, this approach is not suitable for bridges with complex geometries. It is interesting to note that component segmentation could be also come true by combining with the deeply understanding of segmented object and point cloud operation. Lu and Brilakis [24] introduced an innovative top-down approach for detecting slab, pier, pier cap, and girder components based on the deeply understanding on the feature of beam-slab bridges. Results from 10 real-world bridge point cloud experiments demonstrate that their method achieves exceptionally high detection performance. However, their method has strong specificity and only works on the certain object. Lu and Brilakis emphasized that their method primarily focuses on beam-slab bridges and may not be accommodated on the nonuniformly distributed points scenarios. Unfortunately, the box girder bridge exhibits distinct superstructure features and a noticeable imbalance in point cloud distribution.

Currently, the most popular approach to semantic segmentation from point cloud data is through point cloud segmentation networks based on deep learning. A pivotal milestone in this domain was the presentation of PointNet in 2017 [31]. PointNet has the distinctive capability of directly utilizing point clouds for bridge segmentation, eliminating the need to transform the point cloud into regular formats, such as 3D voxel grids or two-dimensional (2D) representations [32], to serve as standard inputs for the network. A significant amount of bridge segmentation work is based on this principle. For instance, Yixiong et al. [33] developed BridgeNet, a 3D deep learning neural network trained on synthetic datasets, automating the segmentation of masonry arch bridges from laser-scanned point clouds and achieving state-of-the-art performance. Daniel et al. [34] introduced a new method for creating synthetic point clouds of truss bridges, and their adapted model from JSNet, trained with these point clouds, demonstrated effective segmentation. Other applications include segmentation of frame, girder, and gravity bridges [35], railway bridges [36], bridges with curved decks or different pier heights [37], dual-track bridges [38], reinforced concrete bridges [39],

highway bridges [40], among others [41].

Once the classified point cloud of the bridge component is obtained, the next step involves geometric feature extraction to facilitate geometric modeling. For cylindrical piers of bridges with regular cross-sections, the RANSAC algorithm [42] or feature matching method [43] can be employed to extract geometric parameters and polygonal cross-section features are typically extracted through slices. However, due to the deviation of the tangent plane setting that would cause contour projection point deformation or overlap, the approach based on slices requires manual control over the tangent plane's verticality and the component's central axis. This manual control is subjective and relatively inefficient.

In the last decades, updating technology has been introduced into the DT of bridges. However, existing literature does not wholly connect the pre-processing phases, segmentation, geometric feature extraction, and model creation for the DT of box girder bridges. Especially, the internal structure of the box girder has been entirely overlooked in automatic modeling [44]. The conventional approach to modeling internal structure typically relies on design drawings for the manual realization of modeling and spatial pose adjustment of the internal structure. This method, however, presents certain limitations in terms of efficiency and adjustment accuracy.

Therefore, this paper aims to develop a solution for automatic modeling as applicable to box girder bridges. The key objectives of this work include: (1) developed a synthetic point cloud generation method and modified loss function of PointNet++ to enhance segmentation performance for the bridge components; (2) proposed a strategy for cross-section selection and established an unordered point sorting algorithm to facilitate the automatic extraction of key points from cross-sections; (3) raised a coordinate system transformation method to automate modeling of the internal structure in the box girder.
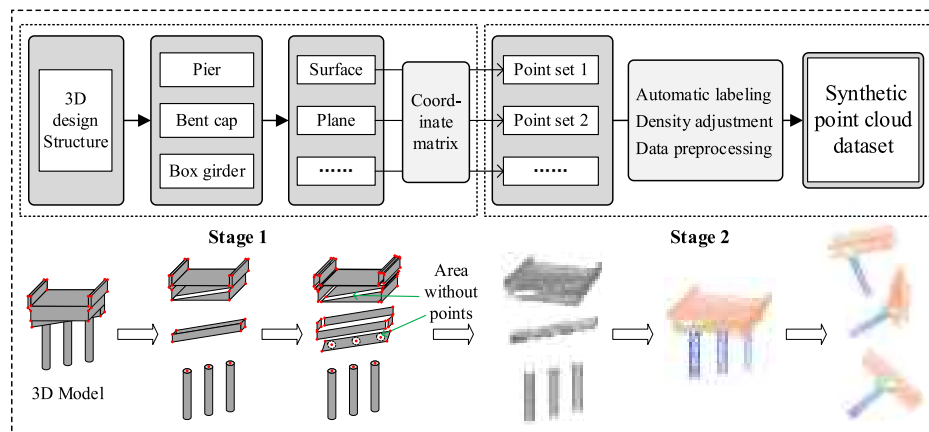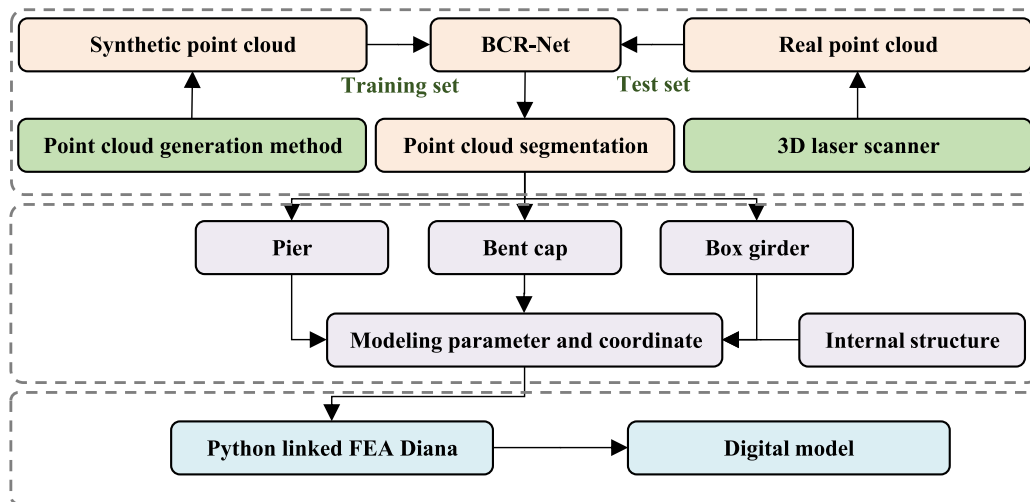
2. Methodology

2.1. Overview

To achieve geometric modeling for digital bridges, the automatic modeling process for the point cloud of the box girder bridge was divided into three vital operations: point cloud segmentation, obtaining key parameters of geometry and coordinates, and reverse modeling. The method's flowchart, illustrated in Fig. 1, displays these operations. Specifically, three components of the box girder bridge - pier, bent cap, and box girder - were initially segmented using BCR-Net, a deep learning-based model proposed in this paper. Following the segmentation, various algorithms were proposed to extract the three components' key geometric and coordinate parameters. Meanwhile, the internal structure of the box girder was mapped to the global coordinate system of the bridge from the designed drawing. Ultimately, the reverse modeling process was executed through Python-linked DIANA, forming an entity model of the digital bridge. Point cloud segmentation and modeling parameters extraction were elaborated in this section.

2.1.1. Synthetic point cloud generated method

The amount of data is a crucial element in deep learning. Hence, we proposed a method for generating point clouds of the box girder to meet the data requirements for the bridge point cloud. The method differs from transforming the macro-integrated 3D model in the software to point cloud. It circumvents the need for solid modeling through software; instead, it relies on delimiting the 3D dimensions of the bridge. It focuses on establishing the 3D model from crucial feature points, and its process unfolds in two stages, as illustrated in Fig. 2.

The prime contribution of Stage 1 lies in constructing a coordinate matrix of geometric vital points. These geometric key points, a set of minimal points capable of describing the geometry (depicted as red points in Fig. 2), are calculated based on the structural form or drawings of box girder bridges. In Stage 1, the 3D model of the bridge is divided

Fig. 1. Automatic processed flowchart.

Fig. 2. Point cloud generation process chart.

into various components, each of which is further subdivided into multiple surfaces, encompassing planes and curves. Each surface functions as a unit to construct a coordinate matrix, and these matrices are then amalgamated to form a comprehensive coordinate matrix for the entire bridge model. It's important to note that the 3D model of the bridge in Fig. 2 is not really constructed but is presented to aid in comprehending the entire method flow. Additionally, a crucial consideration is that some hollow regions exist in the interior of the point cloud obtained by 3D scanning. Therefore, certain surfaces must be provided with a point-free distribution area so that the subsequently generated point clouds can be seamlessly spliced together, forming a standardized internal hollow point cloud model.

The coordinate matrix served to define the surface boundary, and the generated point cloud adhered to a defined coordinate distribution law, represented by Eq. (1). Besides, to simulate the point cloud collected by 3D scanning, all points were discretized and introduced minor errors. Taking the side surface of a bridge pier as an example, considering a pier with a radius of R and height of H, the coordinate distribution equation can be established as follows:

$$\begin{cases} x_i = R \times cos\theta_i, y_i = R \times sin\theta_i, z_i = H \times \theta_i, i = 0, 1, 2, \ldots, n, \\ X = [x_1, x_2, \ldots, x_n]^T, Y = [y_1, y_2, \ldots, y_n]^T, Z = [z_1, z_2, \ldots, z_n]^T, \\ A = [X, Y, Z] \end{cases} \quad (1)$$

Where x_i, y_i, and z_i are the 3D coordinates of the i-th point in the pier point cloud, θ_i is a random angle between 0 and 2π, and n is the number

of points in the point cloud. X, Y, and Z are the vectors composed of three axises coordinates of the pier point cloud, respectively. A is the coordinate matrix of the pier point cloud. Other planes or curved surfaces construct corresponding coordinate matrices based on the same law and different coordinate equations. Each bridge component corresponds to a different set of coordinate matrixes.

In Stage 2, the synthetic dataset of the bridge was generated based on the above coordinate matrixes. To keep the point density of each surface similar, the number of points was associated with the area of the region corresponding to the generated point cloud. This paper set the number of points corresponding to a certain plane of area 100*100 (mm²) as 10,000. In addition, for the surfaces with the same size but different locations, we generated one point cloud of them, and others could get by the transformation of coordinates. The combination of point sets on all surfaces constitutes the point cloud of bridges.

The annotation of the dataset is indispensable for deep learning. The traditional annotation method involves manually selecting the point cloud and adding labels in point cloud visualization software, such as CloudCompare. This process is time-consuming and demanding, and the accuracy of the annotation completely depends on the experience of the operators. However, the annotation method of synthetic point cloud is simultaneously generating label during the synthetic point cloud generating, according to the data format feature and prior knowledge of synthetic point cloud. In contrast to the traditional annotated method, it avoided human error and considerably saved time. In details, the data

format of point cloud includes seven numbers. The first three columns sequentially represent the coordinates x, y, and z. The fourth to sixth columns represent the normal vector and the last column is the label. Hence, the process of annotation on the synthetic point cloud involves adding a number as a label at seventh column for each point. In this paper, the number 0, 1, and 2 indicates pier, bent cap, and box girder, respectively.

The last process of building the dataset is a standardized preprocess of data. Based on the coordinate range, the point clouds of the bridge were cut into multiple samples in the horizontal or vertical direction to extract features better on the proper number of points. The curvature-based down-sampling strategy was employed to adjust the point count to match the model's processing requirements [45,46]. Normalization and augmentation of data were used to improve the convergence speed and promote the model's generalization, respectively.

2.1.2. BCR-net and evaluation metrics

To overcome data imbalance due to the different sizes of bridge components and the problem of accurate segmentation of component joints, a bridge component recognition network (BCR-Net) was proposed based on the focal loss function [47] and PointNet++ [48]. As shown in Fig. 3, the BCR-Net architecture consists of a hierarchical point set feature learning network and a segmentation network.

The feature extraction layer consists of three sublayers: sampling, grouping, and PointNet. The input to the feature extraction layer of the first set of point sets is $(N, (d + C))$, where N is the number of input points, d is the coordinate dimension, and C is the feature dimension. The output is $(N_1, (d + C_1))$, where N_1 is the number of output points, d is the constant coordinate dimension, and C_1 is the new feature size. The sampling layer samples the input points using the farthest point sampling algorithm to select the centroid point. The grouping layer divides all points into several regions based on the chosen centroid points, and it uses the ball query algorithm to generate N_1 corresponding local areas for the points sampled by the sampling layer. After the sampling and grouping layers, all points are divided into overlapping local regions. The PointNet layer encodes each region obtained above into a feature vector to complete point set feature extraction. In the PointNet, the input is $(N_1, K_1, (d + C))$, and the output is $(N_1, (d + C_1))$. Note that local features (shallow features) are extracted in a small range after the first point set feature extraction. After the second feature extraction, higher-level features are extracted based on shallow features in a larger range. The segmentation network is mainly composed of interpolation and PointNet. First, interpolation returns the global features to the previous level points. After the interpolation, the feature point data (interpolated feature) on the corresponding level is obtained, and feature skip link concatenation is performed with the point feature of the set abstraction layer. Finally, PointNet is used as a feature extractor to calculate the corresponding score for each point to achieve classification, that is, to complete the bridge point cloud segmentation.

As mentioned above, the focal loss function was introduced as the loss function to replace the Nll-loss function of PointNet++ for adapting the dataset of the bridge. The focal loss function is represented by Eq. (2) and Eq. (3):

$$FL(p_t) = -\alpha_t (1 - p_t)^\gamma log(p_t) \tag{2}$$

$$
\begin{cases}
p_t = \begin{cases} p_1 & \text{if } y = 0 \text{ (pier)} \\ p_2 & \text{if } y = 1 \text{ (bent cap)} \\ 1 - p_1 - p_2 & \text{if } y = 2 \text{ (box girder)} \end{cases} \\
\alpha_t = \begin{cases} \alpha_1 & \text{if } y = 0 \text{ (pier)} \\ \alpha_2 & \text{if } y = 1 \text{ (bent cap)} \\ 1 - \alpha_1 - \alpha_2 & \text{if } y = 2 \text{ (box girder)} \end{cases}
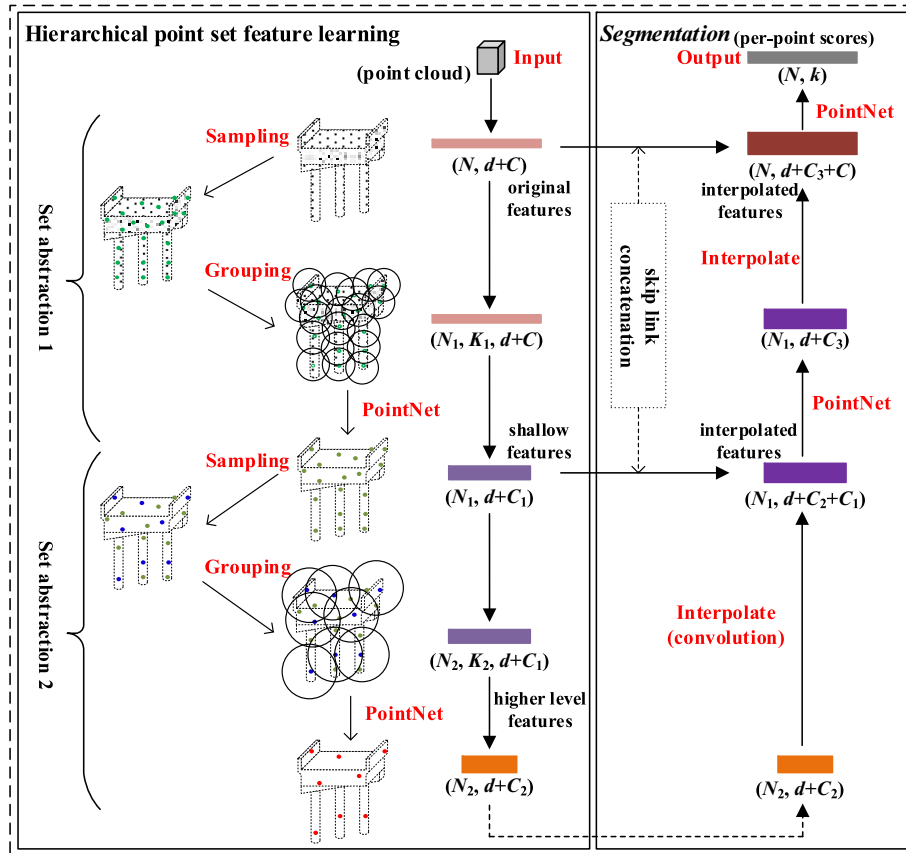\end{cases} \tag{3}
$$

Fig. 3. Feature extraction process using BCR-Net's hierarchical structure.

P_t represents the probability that a certain point is predicted to be a certain bridge component. The probabilities corresponding to the pier, bent cap, and box girder of the bridge are P_1, P_2, and P_3. At the same time, the coefficient α_t is added before the loss function, and the coefficients are α_1, α_2, and α_3, which correspond to the predicted probability of each bridge component. In this way, the contribution of samples to the loss function, such as bridge pier, bent cap, and box girder, can be controlled by setting α_t, thereby solving the problem of unbalanced samples of various components in the bridge point cloud. In addition, for a sample point, the greater the probability that it belongs to a certain class of parts, the easier it is to categorize. Aiming at the characteristics of points that are difficult to classify and easy to classify, the concept of modulation factor is introduced: $(1-P_t)^\gamma$. As P_t tends to be 0, it is difficult to classify, and the modulation factor tends to be 1, significantly contributing to the total loss. When P_t tends to 1, it is easy to classify, and the modulation factor tends to 0, making little contribution to the total loss. The loss contribution weights of easy-to-classify and hard-to-classify samples can be controlled by modulating the factor. Taking advantage of this modulation factor, it is possible to improve the hard-to-classify situation at the connection of bridge components.

To validate the segmentation performance of BCR-Net, PointNet++ was trained simultaneously using the same dataset and operation. Mean accuracy (*MA*) and mean intersection over union (*mIoU*) were used to evaluate the model performance. The equations are listed as follows:

$$MA = \frac{\sum_{i=1}^{n}\left(\frac{TP_i}{TP_i+FN_i}\right)}{n} \tag{4}$$

$$mIoU = \sum_{i=1}^{n}\left(\frac{TP_i}{TP_i+FP_i+FN_i}\right)\bigg/ n \tag{5}$$

Where n is the number of points, and TP_i, FP_i, and FN_i represent the predicted true positives, false positives, and false negatives, respectively.

2.2. Extraction method of modeling parameters

The box girder bridge was divided into three primary components: pier, bent cap, and box girder. Fitting cylindrical piers is easy using the RANSAC algorithm [49], allowing for extracting modeling parameters like center coordinates and diameter for each pier. However, the extraction of bent caps and box girders, which have relatively complex shapes, requires the development of a novel method. Additionally, the point cloud loss of the internal structure of box girders impedes the constructed model with important internal features. This section outlines solutions to these two challenges.

2.2.1. Bent caps and external structure of box girders
To reverse model the bent cap and the external structure of the box girder, a common approach involves stretching and sweeping the cross-section. Addressing the extraction of key points from the cross-section outline consists of steps, including selecting the cross-section, extracting the outline, and confirming key points.

We proposed a cross-section selection strategy where cross-sections above the pier were chosen as benchmark sections. The coordinates of these benchmark sections are based on the coordinates of the pier obtained through the RANSAC algorithm mentioned earlier. Subsequently, cross-section contour points were acquired through slicing. However, these points were disordered and included internal stray points, making them inadequate for precisely describing the cross-section contour. Hence, the Alpha-Concave algorithm [50] and the sorting algorithm based on point distances were introduced to extract and sort external boundary points, respectively. To enhance the modeling speed, an angle-based threshold algorithm was presented to retain the points forming an angle less than 154.7 degrees with their neighboring two points. The

extraction process of cross-section key points is shown in Fig. 4.

2.2.2. Internal structure of box girders
As mentioned above, traditionally, adding the internal structure of the box girder to the model relied on design drawings and manual spatial pose adjustments. However, the size of the design drawings might deviate significantly from the actual dimensions during manual modeling. Therefore, we proposed a coordinate system transformation method based on the Rodrigues algorithm [51] for high-efficiency modeling. This method facilitates automatic and scale-adaptive modeling without manual spatial pose adjustments.

The most significant contribution is building the relationship between the design drawing coordinate system and the global model coordinate system. The two coordinate systems were first assumed, as shown in Fig. 5. The z_1 could be transformed to z_2 as follows equation:

$$\mathbf{z_2} = cos\theta \mathbf{z_1} + (1-cos\theta)(\mathbf{z_1}\cdot\mathbf{K}) + sin\theta\mathbf{K}\times\mathbf{z_1} \tag{6}$$

Where $\mathbf{z_1}$ and $\mathbf{z_2}$ are the unit vectors of Z_1 and Z_2, respectively, $\mathbf{K}$ is the cross product of $\mathbf{z_1}$ and $\mathbf{z_2}$, and θ is the angle between the two axes.

According to Rodrigues algorithm, the rotation matrix $\mathbf{R_1}$ corresponding to the *Z*-axis direction conversion could be calculated by:

$$\mathbf{R} = \mathbf{E}cos\theta + (1-cos\theta)\begin{pmatrix} k_x \\ k_y \\ k_z \end{pmatrix}\begin{pmatrix} k_x & k_y & k_z \end{pmatrix} + sin\theta\begin{pmatrix} 0 & -k_z & k_y \\ k_z & 0 & -k_z \\ -k_y & k_x & 0 \end{pmatrix} \tag{7}$$

Where k_x, k_y, and k_z are the components of $\mathbf{K}$ in three directions; $\mathbf{E}$ is the unit matrix. The X-axis was operated by the same method as the Z-axis to get $\mathbf{R_2}$. Next, based on the original points of two axes, the translation vector $\mathbf{T}$ was calculated to realize the coordinate system position registration. Finally, based on obtaining $\mathbf{R_1}$, $\mathbf{R_2}$, and $\mathbf{T}$, automatically mapping coordinate points of internal structure from the design drawings to the global coordinate system was realized based on the following formulas:

$$\mathbf{Q_2} = \mathbf{Q_1}\cdot\mathbf{R_1}\cdot\mathbf{R_2} + \mathbf{T} \tag{8}$$

Where $\mathbf{Q_1}$ represents a set of points on the design drawing with the Z-coordinate of each point set to 0, and $\mathbf{Q_2}$ is a set of coordinates after $\mathbf{Q_1}$ was mapped to the global coordinate system.

3. Experiment validation

3.1. Building dataset

The synthetic datasets, partly depicted in Fig. 6, were utilized as both the training and verification set for the BCR-Net. A total of 40 artificial point clouds of bridges were generated, of which 30 were used as the
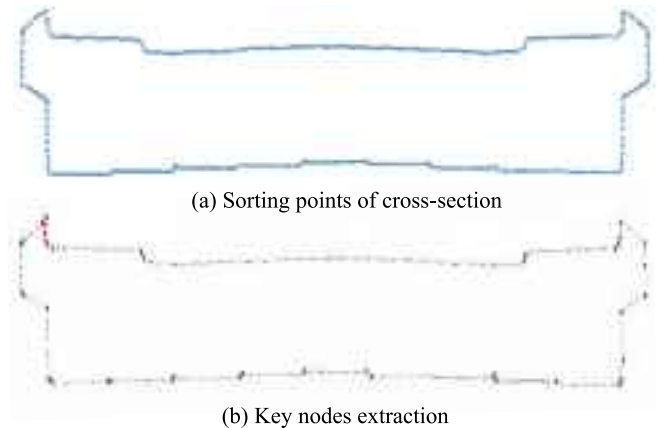

(a) Sorting points of cross-section

(b) Key nodes extraction

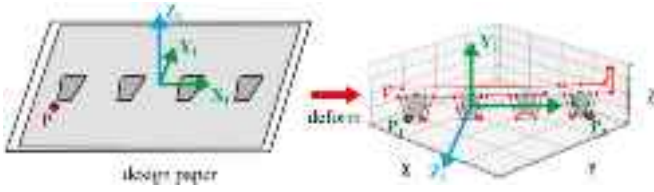**Fig. 4.** Cross-section key points extraction.

Fig. 5. Coordinate system transformation.

training set and 15 as the validation set. After cutting data preprocessing, 240 and 120 samples are in the training and validation sets. Partially scanned point clouds of three in-service bridges consist of the test set, as shown in Fig. 7. A total of 57 samples were obtained through cutting data preprocessing. The details of the dataset are listed in Table 1.

Bridge 1 is a two-way, four-lane elevated line bridge. This section includes 20 cylindrical piers, five main girders, and bridge decks. It is located at the 616 county road section of the No. 12 bridge in Hetianxi section, Quzhou City, Zhejiang Province, and the point cloud was acquired by FARO Focuss350 laser scanner. Bridge 2 is a one-way, two-lane flyover bridge, and this section includes nine cylindrical piers, three inclined girders, and bridge decks. Bridge 3 is a two-way, four-lane flyover bridge; this section contains 12 square piers and bridge decks without main girders. Bridge 2 and Bridge 3 are located in London County, England [52].

For the scanned point cloud of box girder bridge, the traditional annotation method was adopted by using the visual software, CloudCompare. The process of labeling point clouds in CloudCompare mainly involves selection and annotation process. During the selection process, use selection tools (like rectangular or polygonal selection) in combination with rotation, zoom, and hide operations to precisely select the required portions of the point cloud. Then, "Scalar fields" tool was used to add a unique label to each selected part by inputting a unique scalar field name and constant value. To keep consist with the synthetic data, the constant 0, 1, and 2 indicates pier, bent cap, and box girder, respectively.

3.2. BCR-Net implement

BCR-Net was trained on a deep learning GPU server (CPU:

Intel®Xeon®CPU E5–2678 v3@ 2.50 GHz, RAM: 64 GB, GPU: NVIDIA RTX 2080 Ti). In the training process, the Adam algorithm was used as the optimizer to update parameters, with a momentum of 0.9 and a weight attenuation factor of 0.0005. The number of iteration epochs is 150, and the batch size was set to 4. As one of the important hyperparameters in model training, the learning rate helps optimize the network parameters through the gradient of the loss function, determining whether the model can converge to the global minimum. Therefore, the StepLR and MultiStepLR methods were selected to adjust learning rates between 0.01 and 0.0001, thus getting models with excellent performance.

3.3. Modeling example

Bridge 1 was selected as an example to elaborate processes of key point extraction and modeling. The detailed dimensional information on Bridge 1 is shown in Fig. 8 (a) and (b). The modeling result using Python-linked DIANA 10.5 is shown in Fig. 8 (c). To rigorously validate the feasibility and precision of the entire method of extracting key modeling parameters, the dimensional description of the box girder bridge component was displayed in Fig. 9. For external structure of box girder, 17 geometric parameters were defined to descript modeling error and 6 parameters for bent cap. It is used for comparison that the errors produced by our method and the method based on design drawing for external structure of box girder and bent cap. However, it bears repeating that the laser scanner can only capture the surface point cloud of the box girder bridge. And there is no method existed to get the real geometric data of internal structure. Due to process of feature matching and coordinate mapping exists certain system error, the errors of internal structure are only defined as the relative difference between geometric data mapped and of design drawing. According to trapezoid shape of internal structure, 3 parameters were used to evaluate the

Table 1
Dataset details.

Dataset	Training set	Validation set	Test set
Generation type	Synthetic	Synthetic	Scanned
The number of bridges	30	15	3
Cutting samples	240	120	57

Fig. 6. Part synthetic point clouds of bridges.

| (a) Bridge 1 | (b) Bridge 2 | (c) Bridge 3 |

Fig. 7. Scanned point clouds of bridges.

(a) Field photo of Bridge 1

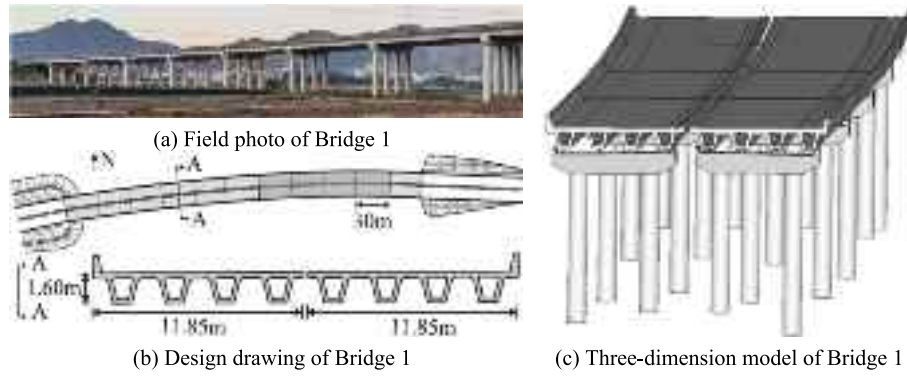(b) Design drawing of Bridge 1   (c) Three-dimension model of Bridge 1

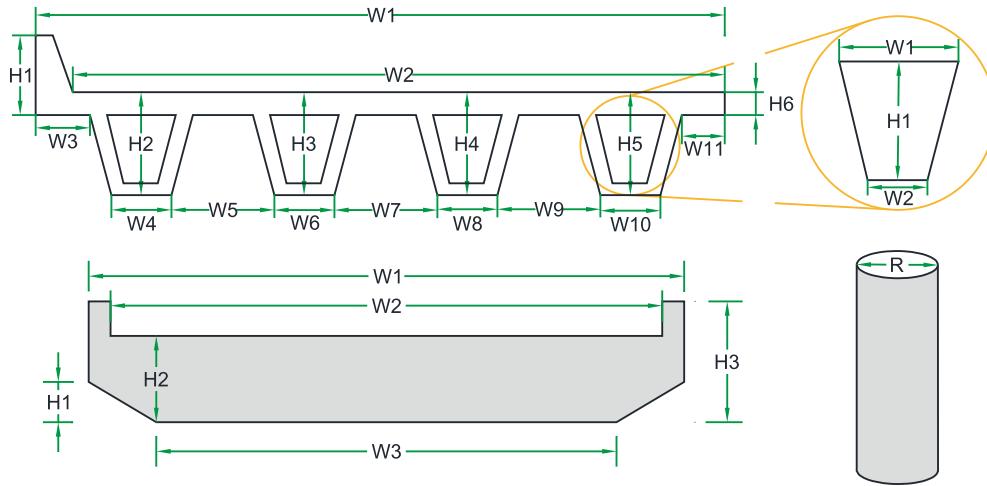**Fig. 8.** Basic information and modeling result of Bridge 1.

Fig. 9. Dimensional description of box girder bridge components.

modeling accuracy of internal structure of box girder. Moreover, it is worth mentioning that the dimensional description of pier only uses the diameter of the cross-section, because the length of piers was uncertain under the earth layer. The results of extracting key feature points and geometric information errors were demonstrated in the next sections.

4. Results and discussion

4.1. BCR-net segmentation performance

MA and mIoU on the test set were recorded after each iteration, as demonstrated in Fig. 10. It is obvious that MA and mIoU, both for BCR-Net and PointNet++, gradually increase in the first 50 epochs and converge to a stable state in the last 100 epochs. Furthermore, the MA of BCR-Net and PointNet++ had reached a maximum of 0.9910 and

Table 2
Summary of validation results of two network models.

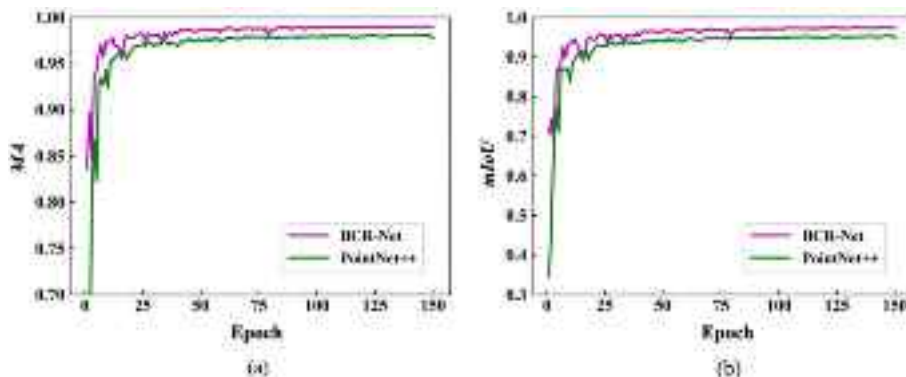| Model	Dataset	Highest *MA*	Highest *mIoU*
BCR-Net	Training set	0.9990	0.9928
	Test set	0.9910	0.9751
PointNet++	Training set	0.9931	0.9698
	Test set	0.9781	0.9536

Fig. 10. (a) MA and (b) mIoU of BCR-Net and PointNet++ on test set during training.

0.9781 on the test set, respectively. mIoU had reached 0.9751 and 0.9536, respectively, as listed in Table 2. The result proved that BCR-Net and PointNet++ can learn the bridge's component features through multi-level point set feature learning. However, the segmentation performance of BCR-Net had a marked increase than PointNet++, which is a benefit from the improvement in the loss function of PointNet++. Namely, the focal loss function is more effective and advantageous than the Nll-loss function on the bridge segmentation with unbalanced data features and difficult classification points. Besides, MA and mIoU on the test set had only decreased slightly compared with the training set, indicating that the point cloud generated by the method proposed in this paper can be a good substitute for the real scan data set in practical applications.

Fig. 11 displays the segmentation results of three bridges in the test set. It is intuitively found that the pier, bent cap, and box girder of three bridges were accurately segmented by BCR-Net. Although the same component had the same semantical information represented by one color, each component has a different size. Hence, the point cloud segmented should be instanced further to facilitate subsequent modeling. DBSCAN algorithm [53] was introduced to realize further segmentation, and the results are shown in Fig. 12.

In a word, the results show that the point cloud segmentation method of bridges based on the BCR-Net architecture proposed in this paper had high recognition accuracy and generalization ability. At the same time, by introducing the DBSCAN algorithm, it was realized the application of bridge point cloud segmentation from component to single instance segmentation.

4.2. Analysis of modeling error on dimensional description

As mentioned above, Bridge 1 was as modeling example for evaluating the validation of the solution proposed. Based on Section 2.3, the RANSAC-based cylinder fitting algorithm extracted the key points of the pier. There 20 piers were fitted and two parameters, length and diameter, were calculated for each pier. Then, the cross-section key points of the bent cap and the external structure of the box girder were extracted by a series of point cloud operations, based on the selecting strategy of cross-section and the extraction method of cross-section key point. We extracted the key points for 10 cross-sections of bent caps, and 10 external structure cross-sections of box girder. These key points of components are shown in Fig. 13. It is extremely obvious that the relative location of the pier with other components and the general outline of the bent cap and external structure of the box girder. Besides, what may be overlooked is the advancement of the whole automatic process. Compared with the traditional manual modeling method based on design drawings, the method proposed, almost without manual interaction, can effectively reduce the deformation error of cross-section outlines and efficiently and accurately construct cross-section points without internal clutter.

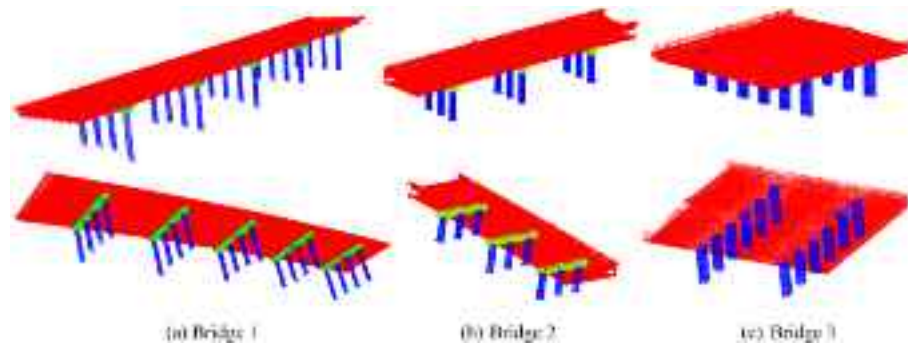The mean relative errors of each component were listed in Table 3

Fig. 12. Segmentation results of (a) piers and (b) bent caps using DBSCAN algorithm.

Fig. 13. Extracted results of key points.

Table 3
Mean absolute error analysis.

Method	Pier	Bent cap	The external structure of the box girder	The internal structure of the box girder
Design drawing-based	0.58 %	1.61 %	5.72 %	–
Our method	0.27 %	0.38 %	0.47 %	0.48 %

and more detailed data was summarized in the supplement material. These errors were calculated using the manual measurements from the point cloud as a baseline, except for the internal structure of the box girder without point cloud data. Thus, the design data is used as a benchmark for it. The comparison of mean absolute error percentages between the two methods, design drawing-based and our method, reveals notable differences in their accuracy in modeling various bridge components. For design drawing-based, the errors are 0.58 % for the pier, 1.61 % for the bent cap, and 5.72 % for the external structure of the box girder. In contrast, our method demonstrates lower errors across all

Fig. 11. Segmentation results of scanned point cloud by BCR-Net. Red points represent box girder, green points represent bent caps, and blue points represent pier. (For interpretation of the references to color in this figure legend, the reader is referred to the web version of this article.)
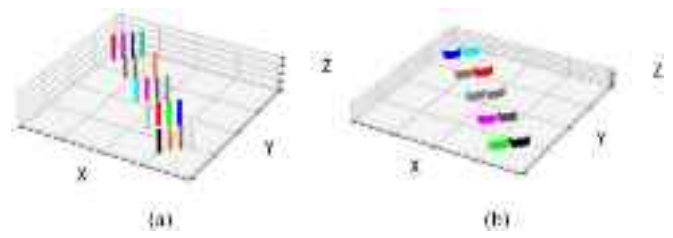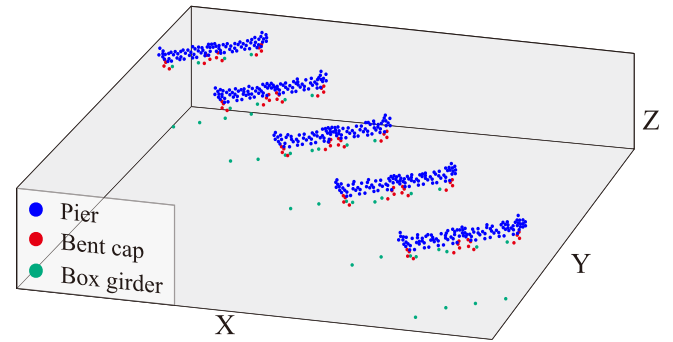
aspects: 0.27 % for the pier, 0.38 % for the bent cap, 0.47 % for the external structure, and 0.48 % for the internal structure of the box girder. Notably, the errors of our method softly increase from the pier to the external structure. The reason could be that the shape characteristics of the component are more complex, and it is difficult to extract its geometry accurately. The error of our method on the internal structure of the box girder also exhibits a relatively low value, 0.48 %, compared with the design drawing.

Further, to elaborate validation of the method and the modeling precision, comparing our method and the method based on design drawing, the mean relative errors of dimensional metrics for each component were plotted as in Fig. 14. It demonstrates the mean relative errors on dimensional metrics of each component using our method are commonly lower than the method based on the design drawing. Besides, error gaps between the two methods are different on various components. The error gap of the pier is less than the bent cap and much less than external structure of box girder. These metrics with large errors are usually concentrated in 'H' which is usually smaller in length. We reasoned that our method performance a more advantages on the small structure than the method based on design drawing. These findings underscore the potential superiority of our method proposed, not only in terms of lower error magnitudes but also in providing a higher modeling efficiency.

4.3. Conclusions

This paper proposes a solution for automatic modeling as applicable to box girder bridges, which addresses the challenge of constructing geometry models that consume significant time and labor. The main contributions include point cloud segmentation, external and internal structure reconstruction, and the conclusion could be summarized as:

(1) This paper presented a synthetic point cloud generation method and a bridge component segmentation network, BCR-Net. Trained on the synthetic dataset, BCR-Net demonstrates strong segmentation performance, achieving a mean accuracy (MA) of over 97 % on real point cloud test sets and a mean intersection over union (mIoU) exceeding 95 %. Compared with PointNet++, BCR-Net shows an improvement of approximately 1.3 % in MA and 2.2 % in mIoU.

(2) The methods proposed accurately extract key points of piers, bent caps and the external structure of box girders. For cylindrical

bridge piers, the RANSAC algorithm is used to fit the cylinder and calculate key parameters, with an average error of only 0.27 % compared to measured geometry. A cross-section selection strategy is proposed to automatically select cross-sections above the pier as benchmark sections for the bent cap and the external structure of the box girder. The Alpha-Concave algorithm and an angle-based threshold algorithm are used to sort cross-section points and filter non-key points, respectively. It is resulting in an average error of 0.38 % and 0.47 % for the bent cap and external structure, respectively.

(3) The internal structures of box girders are accurately reconstructed using a coordinate transformation method that maps the internal structure from design drawings to the 3D modeling space. The margin of error for the mapped internal structure is 0.48 %.

In summary, the proposed solution offers a robust approach for the digital twin of box girder bridges and established a foundation for creating digital models of the infrastructures include internal structures.

While this paper has presented a solution to complete the automatic modeling of box girder bridges, a challenge persists in that instances of each component cannot be directly obtained from the segmentation network. As existing research focuses more on semantic segmentation rather than instance segmentation, future work should explore an instance segmentation network to enhance the precision and efficiency of the modeling process by directly identifying every instance of each component.

CRediT authorship contribution statement

Jiangpeng Shu: Writing – review & editing, Supervision, Resources, Funding acquisition. **Ziyue Zeng:** Writing – original draft, Project administration, Methodology, Conceptualization. **Wenhao Li:** Visualization, Validation, Methodology, Formal analysis, Data curation. **Shukang Zhou:** Writing – original draft, Validation, Resources, Methodology, Formal analysis, Data curation. **Congguang Zhang:** Writing – review & editing, Methodology. **Caie Xu:** Supervision. **He Zhang:** Supervision.
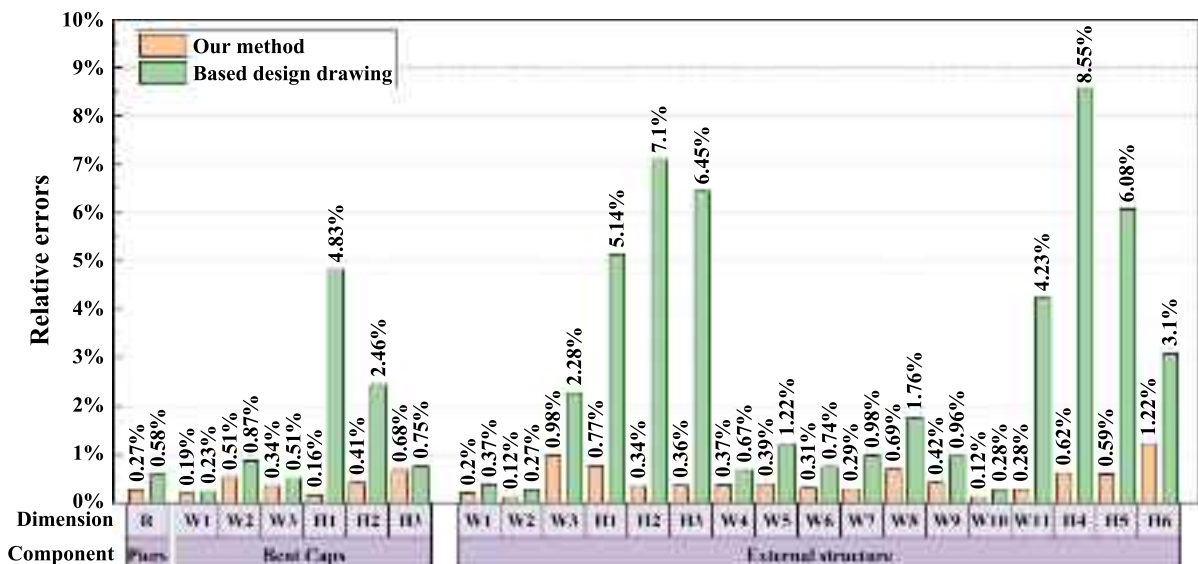
Fig. 14. Relative error comparison.

Declaration of generative AI and AI-assisted technologies in the writing process

During the preparation of this work the authors used ChatGPT in order to improve language. After using this tool, the authors reviewed and edited the content as needed and take full responsibility for the content of the publication.

Declaration of competing interest

The authors declare that they have no known competing financial interests or personal relationships that could have appeared to influence the work reported in this paper.

Data availability

No data was used for the research described in the article.

Acknowledgements

References

[1] A. Velniciuc, C. Bujoreanu, Some analyzes on box girders bridges-literature review, in: IOP Conference Series: Materials Science and Engineering, IOP Publishing, 2022, p. 012039, https://doi.org/10.1088/1757-899X/1262/1/012039.

[2] B. Li, Y. Nie, J. Zhang, J. Jian, H. Gao, Temperature field of long-span concrete box girder bridges in cold regions: testing and analysis, Structures 61 (2024) 105969, https://doi.org/10.1016/j.istruc.2024.105969.

[3] J. Zhang, C.-X. Qu, T.-H. Yi, H.-N. Li, Y.-F. Wang, X.-D. Mei, Detecting deck damage in concrete box girder bridges using mode shapes constructed from a moving vehicle, Eng. Struct. 305 (2024) 117726, https://doi.org/10.1016/j.engstruct.2024.117726.

[4] T. Tao, H. Wang, Q. Zhu, Z. Zou, J. Li, L. Wang, Long-term temperature field of steel-box girder of a long-span bridge: measurement and simulation, Eng. Struct. 236 (2021) 111924, https://doi.org/10.1016/j.engstruct.2021.111924.

[5] M. Abedin, A.B. Mehrabi, Health monitoring of steel box girder bridges using non-contact sensors, Structures 34 (2021) 4012–4024, https://doi.org/10.1016/j.istruc.2021.10.021.

[6] J. Yang, J. Shu, J. Li, K. Yu, K. Zandi, Y. Bai, Experimental study of the influence of inclined pre-cracks on shear behavior of RC beams without transverse reinforcement, Eng. Struct. 299 (2024) 117133, https://doi.org/10.1016/j.engstruct.2023.117133.

[7] C. Zhang, J. Shu, H. Zhang, et al., Estimation of load-carrying capacity of cracked RC beams using 3D digital twin model integrated with point clouds and images, Eng. Struct. 310 (2024) 118126, https://doi.org/10.1016/j.engstruct.2024.118126.

[8] H.H. Hosamo, M.H. Hosamo, Digital twin technology for bridge maintenance using 3D laser scanning: a review, Adv. Civil Eng. 2022 (2022) e2194949 doi:10/gspbg8.

[9] Q. Wang, M.-K. Kim, Applications of 3D point cloud data in the construction industry: a fifteen-year review from 2004 to 2018, Adv. Eng. Inform. 39 (2019) 306–319, doi:10/gspfgf.

[10] H. Hamledari, E. Rezazadeh Azar, B. McCabe, IFC-based development of as-built and as-is BIMs using construction and facility inspection data: site-to-BIM data transfer automation, J. Comput. Civ. Eng. 32 (2018) 04017075 doi:10/gcwrgz.

[11] C. Kim, C.T. Haas, K.A. Liapi, Rapid, on-site spatial information acquisition and its use for infrastructure operation and maintenance, Autom. Constr. 14 (2005) 666–684, doi:10/chqdf6.

[12] Z. Ma, S. Liu, A review of 3D reconstruction techniques in civil engineering and their applications, Adv. Eng. Inform. 37 (2018) 163–174, doi:10/gdx49f.

[13] C. Wang, Y.K. Cho, C. Kim, Automatic BIM component extraction from point clouds of existing buildings for sustainability applications, Autom. Constr. 56 (2015) 1–13, doi:10/gf3952.

[14] X. Xiong, A. Adan, B. Akinci, D. Huber, Automatic creation of semantically rich 3D building models from laser scanner data, Autom. Constr. 31 (2013) 325–337, doi:10/gfc66s.

[15] J. Shu, W. Li, C. Zhang, Y. Gao, Y. Xiang, L. Ma, Point cloud-based dimensional quality assessment of precast concrete components using deep learning, J. Build. Eng. 70 (2023) 106391, https://doi.org/10.1016/j.jobe.2023.106391.

[16] W. Zhao, Y. Jiang, Y. Liu, J. Shu, Automated recognition and measurement based on three-dimensional point clouds to connect precast concrete components, Autom. Constr. 133 (2022) 104000, https://doi.org/10.1016/j.autcon.2021.104000.

[17] J Shu, C. Zhang, K. Yu, M. Shooshtarian, P Liang, IFC-based semantic modeling of damaged RC beams using 3D point clouds, Structural Concrete 24 (1) (2022) 389–401, https://doi.org/10.1002/suco.202200273.

[18] F. Dai, M. Lu, Three-dimensional modeling of site elements by analytically processing image data contained in site photos, J. Constr. Eng. Manag. 139 (2013) 881–894, doi:10/f4589w.

[19] C. Wang, Y.K. Cho, Smart scanning and near real-time 3D surface modeling of dynamic construction equipment from a point cloud, Autom. Constr. 49 (2015) 239–249, doi:10/f6vsk5.

[20] E. Valero, A. Adán, F. Bosché, Semantic 3D reconstruction of furnished interiors using laser scanning and RFID technology, J. Comput. Civ. Eng. 30 (2016) 04015053 doi:10/f8srhh.

[21] H. Son, C. Kim, Automatic segmentation and 3D modeling of pipelines into constituent parts from laser-scan data of the built environment, Autom. Constr. 68 (2016) 203–211, doi:10/f8vhwm.

[22] I. Lubowiecka, J. Armesto, P. Arias, H. Lorenzo, Historic bridge modelling using laser scanning, ground penetrating radar and finite element methods in the context of structural dynamics, Eng. Struct. 31 (2009) 2667–2676, doi:10/bvq6b3.

[23] A. Bhatla, S.Y. Choe, O. Fierro, F. Leite, Evaluation of accuracy of as-built 3D modeling from photos taken by handheld digital cameras, Autom. Constr. 28 (2012) 116–127, doi:10/gtbc8x.

[24] R. Lu, I. Brilakis, C.R. Middleton, Detection of structural components in point clouds of existing RC bridges, Comput. Aided Civ. Inf. Eng. 34 (2019) 191–212, doi:10/gjgnc7.

[25] M. Rashidi, M. Mohammadi, S. Sadeghlou Kivi, M.M. Abdolvand, L. Truong-Hong, B. Samali, A decade of modern bridge monitoring using terrestrial laser scanning: review and future directions, Remote Sens. 12 (2020) 3796, https://doi.org/10.3390/rs12223796.

[26] S.B. Walsh, D.J. Borello, B. Guldur, J.F. Hajjar, Data processing of point clouds for object detection for structural engineering applications, Comput. Aided Civ. Inf. Eng. 28 (2013) 495–508, https://doi.org/10.1111/mice.12016.

[27] A.-V. Vo, L. Truong-Hong, D. Laefer, M. Bertolotto, Octree-based region growing for point cloud segmentation, ISPRS J. Photogramm. Remote Sens. 104 (2015), https://doi.org/10.1016/j.isprsjprs.2015.01.011.

[28] A. Dimitrov, R. Gu, M. Golparvar-Fard, Non-uniform B-spline surface fitting from unordered 3D point clouds for as-built modeling, Comput. Aided Civ. Inf. Eng. 31 (2016) 483–498, https://doi.org/10.1111/mice.12192.

[29] M.-M. Sharif, M. Nahangi, C. Haas, J. West, Automated model-based finding of 3D objects in cluttered construction point cloud models, Comput. Aided Civ. Inf. Eng. 32 (2017) 893–908, https://doi.org/10.1111/mice.12306.

[30] R. Schnabel, R. Wahl, R. Klein, Efficient RANSAC for point-cloud shape detection, Comp. Graph. Forum 26 (2007) 214–226, https://doi.org/10.1111/j.1467-8659.2007.01016.x.

[31] R.Q. Charles, H. Su, M. Kaichun, L.J. Guibas, PointNet: deep learning on point sets for 3D classification and segmentation, in: 2017 IEEE Conference on Computer Vision and Pattern Recognition (CVPR), 2017, pp. 77–85, https://doi.org/10.1109/CVPR.2017.16.

[32] Y. Narazaki, V. Hoskere, T.A. Hoang, B.F. Spencer Jr., Automated vision-based bridge component extraction using multiscale convolutional, Neural Netw. (2018), https://doi.org/10.48550/arXiv.1805.06042.

[33] Y. Jing, B. Sheil, S. Acikgoz, Segmentation of large-scale masonry arch bridge point clouds with a synthetic simulator and the BridgeNet neural network, Autom. Constr. 142 (2022) 104459, https://doi.org/10.1016/j.autcon.2022.104459.

[34] D. Lamas, A. Justo, M. Soilán, B. Riveiro, Automated production of synthetic point clouds of truss bridges for semantic and instance segmentation using deep learning models, Autom. Constr. 158 (2024) 105176, https://doi.org/10.1016/j.autcon.2023.105176.

[35] H. Kim, C. Kim, Deep-learning-based classification of point clouds for bridge inspection, Remote Sens. 12 (2020) 3757, doi:10/gpt9sv.

[36] J.S. Lee, J. Park, Y.-M. Ryu, Semantic segmentation of bridge components based on hierarchical point cloud model, Autom. Constr. 130 (2021) 103847, https://doi.org/10.1016/j.autcon.2021.103847.

[37] H. Kim, J. Yoon, S.-H. Sim, Automated bridge component recognition from point clouds using deep learning, Struct. Control. Health Monit. 27 (2020) e2591, https://doi.org/10.1002/stc.2591.

[38] J. Li, Y. Peng, Z. Tang, Z. Li, Three-dimensional reconstruction of railway bridges based on unmanned aerial vehicle–terrestrial laser scanner point cloud fusion, Buildings 13 (2023) 2841, doi:10/gtcq86.

[39] X. Yang, E. del Rey Castillo, Y. Zou, L. Wotherspoon, Semantic segmentation of bridge point clouds with a synthetic data augmentation strategy and graph-structured deep metric learning, Autom. Constr. 150 (2023) 104838 doi:10/gtcq84.

[40] Y.-C. Lin, A. Habib, Semantic segmentation of bridge components and road infrastructure from mobile LiDAR data, ISPRS Open J. Photogram. Remote Sens. 6 (2022) 100023 doi:10/gtcq85.

[41] M.S. Mafipour, C. Alici, S.S. Shakeel, A. Kalkavan, Semantic segmentation of real and synthetic point cloud data for digital twinning of bridges, in: Proceedings of 33. Forum Bauinformatik, 2022.

[42] K.G. Derpanis, Overview of the RANSAC Algorithm, 2024.

[43] Y. Yu, H. Guan, D. Li, S. Jin, T. Chen, C. Wang, J. Li, 3-D feature matching for point cloud object extraction, IEEE Geosci. Remote Sens. Lett. 17 (2020) 322–326, https://doi.org/10.1109/lgrs.2019.2918073.

[44] L. Truong-Hong, R. Lindenbergh, Extracting bridge components from a laser scanning point cloud, in: E. Toledo Santos, S. Scheer (Eds.), Proceedings of the 18th International Conference on Computing in Civil and Building Engineering, Springer

International Publishing, Cham, 2021, pp. 721–739, https://doi.org/10.1007/978-3-030-51295-8_50.

[45] H. He, Y. Bai, E.A. Garcia, S. Li, ADASYN: adaptive synthetic sampling approach for imbalanced learning, in: 2008 IEEE International Joint Conference on Neural Networks (IEEE World Congress on Computational Intelligence), 2008, pp. 1322–1328, doi:10/c7rh62.

[46] D. Griffiths, J. Boehm, Weighted Point Cloud Augmentation for Neural Network Training Data Class-Imbalance, arXiv.Org, 2019, https://doi.org/10.5194/isprs-archives-XLII-2-W13–981-2019.

[47] T.-Y. Lin, P. Goyal, R. Girshick, K. He, P. Dollár, Focal Loss for Dense Object Detection, 2018, https://doi.org/10.48550/arXiv.1708.02002.

[48] C.R. Qi, L. Yi, H. Su, L.J. Guibas, PointNet++: Deep hierarchical feature learning on point sets in a metric space, in: I. Guyon, U.V. Luxburg, S. Bengio, H. Wallach, R. Fergus, S. Vishwanathan, R. Garnett (Eds.), Advances in Neural Information

Processing Systems, Curran Associates, Inc., 2017, in: https://proceedings.neurips.cc/paper_files/paper/2017/file/d8bf84be3800d12f74d8b05e9b89836f-Paper.pdf.

[49] M.A. Fischler, R.C. Bolles, Random sample consensus: a paradigm for model fitting with applications to image analysis and automated cartography, Commun. ACM 24 (1981) 381–395, doi:10/d4x75c.

[50] S. Asaeedi, F. Didehvar, A. Mohades, α-Concave hull, a generalization of convex hull, Theor. Comput. Sci. 702 (2017) 48–59, doi:10/gcs325.

[51] J.E. Mebius, Derivation of the Euler-Rodrigues formula for three-dimensional rotations from the general formula for four-dimensional rotations, arXiv.Org, 2007, https://arxiv.org/abs/math/0701759v1 (accessed January 8, 2024).

[52] R. Lu, I. Brilakis, Digital twinning of existing reinforced concrete bridges from labelled point clusters, Autom. Constr. 105 (2019) 102837 doi:10/ghg9s7.

[53] M. Ester, H.-P. Kriegel, J. Sander, X. Xu, et al., A density-based algorithm for discovering clusters in large spatial databases with noise, in: KDD, 1996, pp. 226–231.